Impaired Lung ^{123}I-MIBG Uptake on SPECT in Pulmonary Emphysema

Kazuyoshi Suga[1], Munemasa Okada[2], Mitsue Kunihiro[2], Osamu Tokuda[2], Hideyuki Iwanaga[2], and Naofumi Matsunaga[2]

[1]Department of Radiology, St. Hill Hospital, Yamaguchi, Japan; and [2]Department of Radiology, Yamaguchi University School of Medicine, Yamaguchi, Japan

The aim of this study was to evaluate impaired lung uptake of ^{123}I-metaiodobenzylguanidine (^{123}I-MIBG) on SPECT, compared with perfusion SPECT and morphologic CT, in patients with pulmonary emphysema (PE). **Methods:** ^{123}I-MIBG SPECT was performed at 15 min and 4 h after intravenous injection of ^{123}I-MIBG in 36 PE patients with a history of smoking and variable-extent low-attenuation areas on CT, indicative of emphysematous changes, and in 16 controls with no history of smoking and no noticeable low-attenuation areas. The distribution of ^{123}I-MIBG was compared with that of low-attenuation areas on CT and perfusion on SPECT at the base of the 180 lung lobes of the PE patients. Total-lung ^{123}I-MIBG kinetics were calculated, including early and delayed lung-to-mediastinum uptake ratios and washout rate. **Results:** The controls showed a fairly uniform lung ^{123}I-MIBG distribution nearly consistent with perfusion. PE patients had heterogeneous ^{123}I-MIBG defects showing frequent discordance with low-attenuation areas or perfusion distribution; ^{123}I-MIBG defects were more extensive than low-attenuation areas in 76 lobes (42.2%) of 31 patients (86%) and more extensive than perfusion defects in 44 lobes (24.4%) of 22 patients (61%). ^{123}I-MIBG defects were seen regardless of the absence of noticeable low-attenuation areas and perfusion defects in 19 lobes (10.5%) of 16 patients (44%). All total-lung ^{123}I-MIBG kinetic parameters in PE patients were significantly lower than the control values ($P < 0.0001$), with significant correlation with alveolar–arterial oxygen tension gradient but without correlation with the extent of perfusion defects or low-attenuation areas. **Conclusion:** ^{123}I-MIBG SPECT allows evaluation of lung pathophysiology in PE independently of perfusion SPECT or morphologic CT, and impairment of lung ^{123}I-MIBG uptake may be more extensive than perfusion or morphologic abnormalities in PE.

Key Words: metaiodobenzylguanidine (MIBG); pulmonary emphysema; single-photon emission computed tomography (SPECT); computed tomography (CT)

J Nucl Med 2011; 52:1378–1384
DOI: 10.2967/jnumed.111.090076

Pulmonary emphysema (PE) is pathologically characterized by progressive disappearance of alveolar structures. Injury of alveolar endothelial cells (AECs) is of great concern and has been considered the primary pathogenesis of PE (*1–11*). Several histopathologic studies have shown early damage of these cells in smokers and mild-PE patients (*2–4,8–10*). Recently, evidence that functional impairment of AECs primarily induces alveolar septal cell apoptosis, leading to emphysematous changes, has been accumulating (*5,8,10,11*).

AECs in the lung microvasculature have the metabolic function of circulating vasoactive norepinephrine (*12–15*). ^{123}I-metaiodobenzylguanidine (^{123}I-MIBG) shares the same uptake as norepinephrine in AECs (*12–15*). ^{123}I-MIBG scintigraphic studies have been used to detect and assess the functional injury or integrity of AECs in various lung diseases, including PE (*16–23*). SPECT provides better assessment of lung ^{123}I-MIBG uptake than planar scanning and allows cross-sectional comparisons with lung morphologic CT scans and perfusion SPECT scans.

In the present study, impaired uptake of ^{123}I-MIBG on cross-sectional SPECT images of the lungs of PE patients was compared with lung morphologic changes on CT and perfusion distribution on SPECT.

MATERIALS AND METHODS

Study Population

The population included 36 PE patients with variable-extent low-attenuation areas on high-resolution chest CT, indicative of emphysematous lungs, and 16 control subjects with no history of smoking and no noticeable low-attenuation areas on CT, who underwent ^{123}I-MIBG SPECT during June 2004 to August 2010 (Table 1). All PE patients had a history of smoking, and PE was diagnosed according to the criteria of the American Thoracic Society (*24,25*). Another 13 PE patients also underwent ^{123}I-MIBG SPECT during the same period, but these patients were excluded because of the presence of concomitant diseases such as hypertension, diabetes mellitus, congestive heart failure, or thyroid disease and drug therapy (such as sympathomimetics, antihypertensive drugs, or tricyclic antidepressants) that may interfere with ^{123}I-MIBG uptake (*2,16,21*). All subjects underwent high-resolution chest CT within 3 wk before or after ^{123}I-MIBG SPECT, as well as ^{99m}Tc-macroaggregated albumin perfusion SPECT within 5–10 d before or after ^{123}I-MIBG SPECT. Alveo-

Received Mar. 4, 2011; revision accepted May 24, 2011.
For correspondence or reprints contact: Kazuyoshi Suga, Department of Radiology, St. Hill Hospital, 3-7-18 Imamurakita, Ube, Yamaguchi 755-0151, Japan.
E-mail: sugar@sthill-hp.or.jp
Published online Aug. 3, 2011.
COPYRIGHT © 2011 by the Society of Nuclear Medicine, Inc.

TABLE 1
Study Population

Characteristic	Data
PE patients	
Sex	29 men and 7 women
Age	62.8 ± 8.6 y (range, 49–83 y)
Smoking history	27 ± 13 pack-years (range, 10–91 pack-years)
%FEV1	75.4% ± 12.4% (range, 42.7%–95.7%)
FEV1	2,328 ± 287 cm^3 (range, 1,284–3,685 cm^3)
%VC	87.6% ± 11.7% (range, 81.7%–115.4%)
A-aDo_2	14.6 ± 9.7 torr (range, 2–36 torr)
Low-attenuation areas*	15.4% ± 7.9% (range, 4.3%–34%)
Perfusion defects†	20.8% ± 7.4% (range, 8.9%–37%)
Controls	
Sex	9 men and 7 women
Age	54 ± 3.1 y (range, 51–62 y)
%FEV1	99.4% ± 2.9% (range, 97.4%−111.7%)
FEV1	3,417 ± 208 cm^3 (range, 2,951–3,882 cm^3)
%VC	95.4% ± 5.7% (range, 95.8%−109.5%)

*Percentage of total-lung voxels with attenuation < −960 HU on CT.

†Percentage of total-lung voxels with radioactivity < 10% of maximum on perfusion SPECT.

%FEV1 = predicted forced expiratory volume in 1 s; FEV1 = forced expiratory volume in 1 s; %VC = predicted vital capacity.

lar–arterial oxygen tension gradient (A-aDo_2) was also measured within 5 wk before or after ^{123}I-MIBG SPECT. On CT, in addition to variable-extent low-attenuation areas, 21 PE patients had scattered, small bullae (<2 cm) predominantly in the lung apex and 11 patients had small old inflammatory scars or old pleuritic lesions predominantly in the lung apex; the remaining 25 patients did not have any concomitant lesions. Perfusion SPECT showed variable-extent perfusion defects in all PE patients.

The 16 nonsmoker controls were selected from relatively young patients who underwent ^{123}I-MIBG or perfusion SPECT and chest CT during the same period. They had experienced temporal chest pain and were being evaluated for suspected ischemic cardiac disease or pulmonary vascular or airway-obstructive disease. These controls had no history of cardiac or lung disease and were finally found to be free of any detectable heart or pulmonary disease on the basis of no noticeable abnormalities on ^{123}I-MIBG or perfusion SPECT and chest CT (and additional ^{201}Tl SPECT in several subjects), with normal findings on physical examination, electrocardiography, echocardiography, pulmonary function testing, and arterial blood gas analysis.

The ^{123}I-MIBG SPECT protocol was approved by the local ethical committee of Yamaguchi University School of Medicine, and written consent was obtained from all subjects after they had been fully informed of the purpose and procedure.

^{123}I-MIBG SPECT

All subjects received 200 mg of potassium perchloride per day orally, starting the day before SPECT and continuing for 2 d, to block uptake by the thyroid. ^{123}I-MIBG (111 MBq) was injected intravenously with the subject resting supine after overnight fasting. SPECT was performed using a dual-head system (E-cam; Toshiba Medical) with a low-energy, high-resolution collimator at 15 min (early scan) and 4 h (delayed scan) after injection of ^{123}I-MIBG. This timing was applied according to previous investigations of lung ^{123}I-MIBG kinetics using planar images obtained 15–20 min and 3–4 h after injection (*23*). Each detector was moved at 6° increments and recorded data from 60 angular directions (360° arc) using a step-and-shoot technique, and projection data (128 × 128 pixels, 3.2 mm/pixel) were acquired. Images were acquired for 20 s per projection for a total imaging time of approximately 20 min, with 20% energy windows centered at a photopeak of 159 keV. SPECT data were reconstructed into multislice images in 3 orthogonal planes throughout the entire lung, using a Butterworth prefilter (cutoff frequency of 0.11 cycles/cm, order of 8) and a ramp backprojection filter, with a slice thickness of 2 pixels (6.4 mm), gapless. The lung contour on ^{123}I-MIBG SPECT images was drawn at a threshold of 10% of the maximum radioactivity of the lungs in each subject.

Perfusion SPECT

After injection of approximately 185 MBq (5 mCi) of ^{99m}Tc-macroaggregated albumin with the subject supine, SPECT was performed using the same system as for the ^{123}I-MIBG scan but with an energy window centered at a photopeak of 140 keV. Three orthogonal-plane images throughout the entire lung were reconstructed using a Butterworth prefilter (cutoff frequency of 0.13 cycles/cm, order of 8) and a ramp filter, with the same slice thickness of 2 pixels (6.4 mm) as for ^{123}I-MIBG SPECT. The lung contour on perfusion SPECT images was drawn at a threshold of 20% of the maximum radioactivity of the lungs in each subject. The extent of perfusion defects in the lung was automatically quantified as the percentage of voxels with radioactivity less than 10% of the maximum radioactivity.

Chest CT

Chest CT was performed using a 16- or 64-detector-row scanner (Somatom Emotion or Sensation; Siemens-Asahi Medical Ltd.). With the subject supine, contiguous 3-mm-interval and 1.5- or 3-mm-thick CT images were obtained in a 512 × 512 matrix during a deep inspiratory breath-hold, with a tube rotation time of 0.8 s, at 120–135 kVp and 200–230 mA. A total of 78–129 transaxial CT images covering the entire lung were reconstructed with the lung algorithm (high-spatial-frequency reconstruction). The lung images were displayed using standard lung window settings (window level, 700 Hounsfield units [HU]; window width, 1,000–1,500 HU). To display the lung distribution of low-attenuation areas indicative of emphysematous lungs, density-mask CT images were created using M900 Quadra imaging software (Zio Soft K.K.). For segmentation of low-attenuation areas on density-mask CT, a threshold of −960 HU was applied, according to previous studies (*26,27*). The density-mask CT used red to indicate low-attenuation areas in the lung. The extent of the low-attenuation area in the lung was automatically quantified as the percentage of voxels with attenuation less than −960 HU.

Image Interpretation and Data Analysis

Two experienced observers working in consensus compared the distribution of ^{123}I-MIBG with that of perfusion on SPECT and low-attenuation areas on density-mask CT at the base of the lobe in each subject. On visual inspection, the severity of lung ^{123}I-MIBG or perfusion defects and low-attenuation areas was classified as limited if the extent was less than 50% of each lobe or as extensive if greater than 50%–60%. In this assessment, the matched transaxial slices of the respective SPECT and CT scans were determined by referring to the scout-view images and the distances from the diaphragm and lung apex. Then, the series of SPECT and CT slices were simultaneously displayed side by side, and adequate correspondence of each lobe was confirmed by comparing the contours of the heart, aorta, and hilar vessels. Any slight mismatching was considered inconsequential because each ^{123}I-MIBG and perfusion defect and low-attenuation area was relatively extensive in size and spread, appearing similar in at least 2 adjacent planes.

For quantitative analysis of lung ^{123}I-MIBG uptake, a summed coronal image of every ^{123}I-MIBG SPECT section in the entire lung was created for each subject. As an index of total-lung ^{123}I-MIBG uptake, early and delayed ratios of lung uptake relative to mediastinal uptake (L/M ratios) were estimated using averaged counts per pixel obtained from regions of interest covering the entire lung on the early and delayed summed coronal SPECT images (*23*). In this assessment, the delayed counts were corrected for ^{123}I decay. In the 11 PE patients with concomitant lesions other than emphysema, the local areas with these lesions were excluded in setting regions of interest. ^{123}I-MIBG washout rate, defined as (early L/M ratio – delayed L/M ratio)/early L/M ratio, was also calculated according to the previous study (*23*). These measurements were independently performed by the 2 observers, and the data were averaged. The number of total-lung radioactivity counts for all subjects ranged from 3,872 to 29,387 (average, 2,853 ± 2,971) on early SPECT and from 2,885 to 29,162 (average, 20,863 ± 2,847) on delayed SPECT.

In PE patients, the correlations of total-lung early and delayed L/M ratios and washout rate with the extent of perfusion defects or low-attenuation areas and with A-aD_{O_2} were evaluated.

Statistical Analysis

Results were expressed as the mean ± SD, and a Mann–Whitney *U* test for nonparametric data was used to analyze differences between controls and PE patients. A probability value of less than 0.05 indicated a significant difference. In PE patients, linear regression analysis was performed to assess the correlations of total-lung early and delayed L/M ratios and washout rate with the extent of perfusion defects or low-attenuation areas and with A-aD_{O_2}, using the commercially available Statview Statistical Package (Abacus Concepts). A probability value of less than 0.05 was considered significant for each correlation coefficient.

RESULTS

All 16 controls showed a homogeneous and symmetric distribution of ^{123}I-MIBG in the lungs on both early and delayed SPECT, but with a gravitational effect showing the most intensive ^{123}I-MIBG uptake in the lower dorsal part of the lungs (Fig. 1). ^{123}I-MIBG distribution appeared nearly consistent with perfusion distribution.

By contrast, all 36 PE patients showed partly or diffusely reduced lung ^{123}I-MIBG uptake, predominantly in the upper lung zones (Figs. 2 and 3). Although variable-extent ^{123}I-MIBG defects were seen in all the lung lobes with low-attenuation areas or perfusion defects, discordance was frequent (Table 2). Extensive ^{123}I-MIBG defects were seen in 76 lobes (42.2%) with limited-extent low-attenuation areas in 31 patients (86%) and in 44 lobes (24.4%) with limited-extent perfusion defects in 22 patients (61%). ^{123}I-MIBG defects were even seen in 19 lobes (10.5%) without noticeable low-attenuation areas or perfusion defects in 16 patients (44%). Although a total of 56 lobes (31.1%) with extensive perfusion defects showed consistently extensive ^{123}I-MIBG defects, faint ^{123}I-MIBG radioactivity was seen in 19 lobes (10.5%) with nearly complete perfusion defects in 19 patients (52%).

Quantitatively, the total-lung delayed L/M ratio was lower than the early ratio in all controls but was higher in 14 PE patients (38%) (Fig. 4). All total-lung early and delayed L/M ratios and washout rates were significantly lower in PE patients than in controls ($P < 0.0001$) (Table 3; Supplemental Fig. 1; supplemental materials are available online only at http://jnm.snmjournals.org). All these ^{123}I-MIBG parameters in these patients had no correlation with the extent of total-lung perfusion defects or low-attenuation areas (not statistically significant). All these ^{123}I-MIBG parameters and the extent of perfusion defects in PE patients were significantly correlated with A-aD_{O_2} (Table 4; Supplemental Fig. 2; Fig. 5), whereas the extent of low-attenuation areas had no correlation.

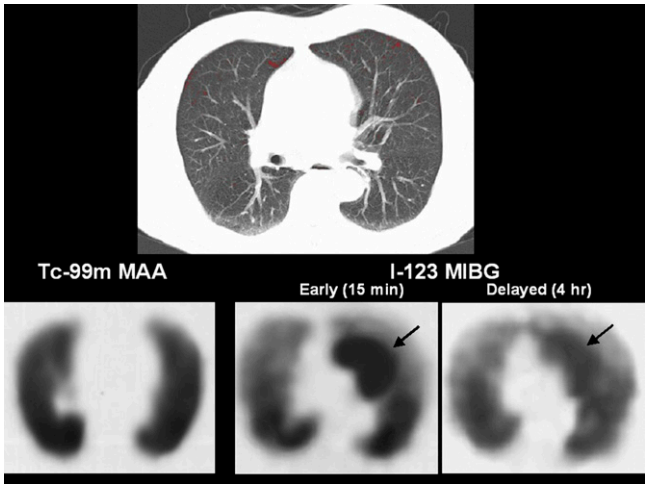

RGB

FIGURE 1. A 58-y-old male control subject. Density-mask CT at lower lung zone (top) shows only few low-attenuation areas < −960 HU (red). Early and delayed ^{123}I-MIBG SPECT at corresponding lung level of CT shows homogeneous and symmetric ^{123}I-MIBG distribution in lung, similar to perfusion distribution on ^{99m}Tc-macroaggregated albumin (MAA) SPECT. Total-lung early L/M ratio, delayed L/M ratio, and washout rate are 4.80, 3.21, and 32.0%, respectively. ^{123}I-MIBG radioactivity in heart is partly seen (arrows).

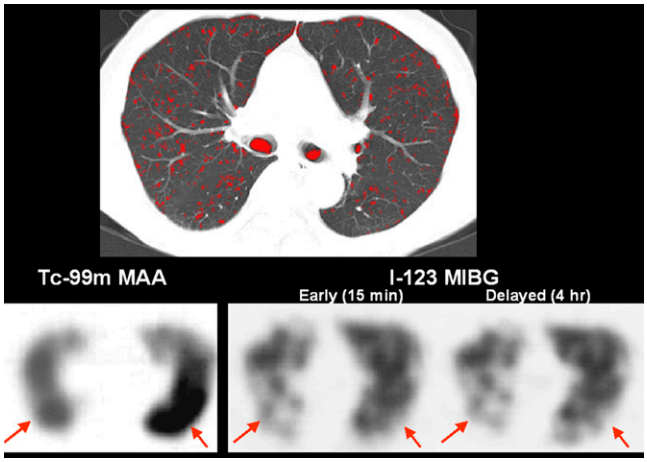

FIGURE 2. A 54-y-old man with mild PE. Density-mask CT at lower lung zone (top) shows scattered low-attenuation areas (red). Early and delayed ^{123}I-MIBG SPECT at corresponding lung level of CT shows reduced and inhomogeneous ^{123}I-MIBG uptake in both lungs, compared with control subject in Figure 1. Some lung parts show apparently reduced ^{123}I-MIBG uptake, compared with perfusion seen on ^{99m}Tc-macroaggregated albumin (MAA) SPECT (arrows). Total-lung early L/M ratio, delayed L/M ratio, and washout rate are 2.21, 1.91, and 13.5%, respectively.

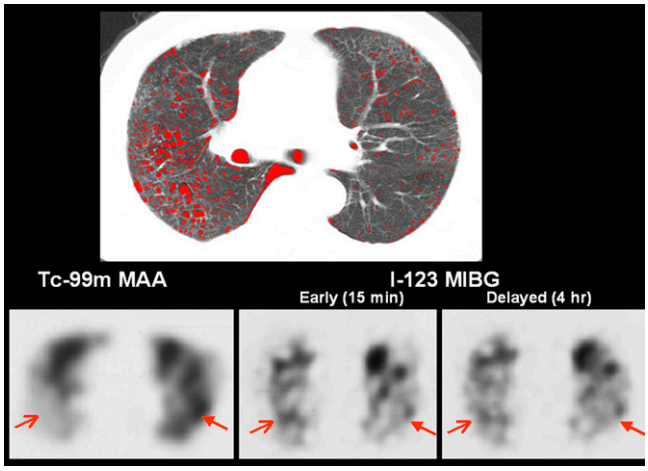

FIGURE 3. A 63-y-old man with relatively advanced PE. Density-mask CT at lower lung zone (top) shows relatively extensive low-attenuation areas in right lung (red). Early and delayed ^{123}I-MIBG SPECT at corresponding lung level of CT shows reduced and inhomogeneous ^{123}I-MIBG uptake in both lungs, compared with control subject in Figure 1. Some lung parts show apparent discordance between ^{123}I-MIBG uptake and perfusion seen on ^{99m}Tc-macroaggregated albumin SPECT (arrows). Total-lung early L/M ratio, delayed L/M ratio, and washout rate are 1.18, 1.15, and 2.5%, respectively.

DISCUSSION

The present study showed a significant reduction of lung ^{123}I-MIBG uptake and washout rate in PE patients, compared with controls. Lung ^{123}I-MIBG defects in these patients were frequently more extensive than perfusion defects or low-attenuation areas at the base of the lobe and were occasionally seen even in lobes without noticeable perfusion defects or low-attenuation areas. The estimated ^{123}I-MIBG kinetic parameters correlated with A-aDo_2 but not with the extent of total-lung perfusion defects or low-attenuation areas. These results indicate that ^{123}I-MIBG SPECT can be an investigative tool to evaluate lung pathophysiology in PE, independently of perfusion SPECT and morphologic CT.

The AECs of the lung extract and metabolize approximately 25%–50% of norepinephrine, that is, ^{123}I-MIBG, during a single pass through pulmonary circulation (*13–15*). The fact that the homogeneous lung ^{123}I-MIBG distribution was nearly consistent with perfusion in our controls appears to be attributable to this high extraction of ^{123}I-MIBG in AECs. The slight variability in estimated lung ^{123}I-MIBG kinetic parameters in our controls is consistent with previous observations on planar ^{123}I-MIBG scintigraphic studies of healthy subjects (*21–23*).

The significant reduction of lung ^{123}I-MIBG uptake in our PE patients can be explained by lack of function and integ-

TABLE 2
Comparison of Lung ^{123}I-MIBG Uptake with Perfusion and Low-Attenuation Areas in PE Patients

Findings	No. of lobes	No. of patients
Preserved ^{123}I-MIBG uptake in lobe, without noticeable perfusion defect and low-attenuation areas	20 (11.1%)	18 (50%)
Limited ^{123}I-MIBG defect in lobe, without noticeable perfusion defect and low-attenuation areas	19 (10.5%)	16 (44%)
Limited ^{123}I-MIBG defect in lobe, with limited perfusion defect and low-attenuation areas	41 (22.7%)	36 (100%)
Extensive ^{123}I-MIBG defects in lobe, with limited perfusion defect and low-attenuation areas	44 (24.4%)	22 (61%)
Extensive ^{123}I-MIBG defects in lobe, with extensive perfusion defect but limited low-attenuation areas	32 (17.7%)*	28 (77%)
Extensive ^{123}I-MIBG defects in lobe, with extensive perfusion defect and low-attenuation areas	24 (13.3%)*	17 (47%)

*All 56 lobes with extensive perfusion defects had extensive ^{123}I-MIBG defects, but in 19 patients (52%) with nearly complete perfusion defects, some faint ^{123}I-MIBG radioactivity was seen in 19 lobes (10.5%).

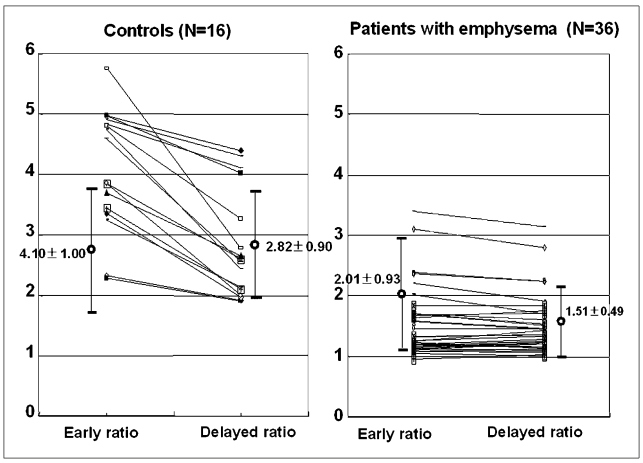

FIGURE 4. Comparison of changes in lung ^{123}I-MIBG uptake on early and delayed SPECT between controls and PE patients. Total-lung delayed L/M ratio is lower than early L/M ratio in all 16 controls but is higher in 14 (38.9%) of 36 PE patients.

rity of the AECs and loss of the pulmonary vascular bed. Pulmonary arterial vasoconstriction due to oxidant or inflammation-induced mediators and regional hypoxia associated with smoking, and vascular compression in emphysematous lungs, induces ischemia and damage to AECs (*12,15,16, 23,28*). Previous histologic studies showed frequent thinning or disappearance of AECs in PE patients (*2–4,8–10,23,29–33*). Damaged AECs cannot efficiently extract circulating ^{123}I-MIBG (*9,12,13,28*). The previous animal model studies of pulmonary vascular damage showed a linear relationship between the degree of reduced ^{123}I-MIBG uptake and loss of the pulmonary vascular bed (*17,23*). Poor delivery of ^{123}I-MIBG due to decreased perfusion also may reduce ^{123}I-MIBG uptake, as ^{123}I-MIBG defects were persistently seen at the lung lobes with perfusion defects in our patients. The occasional ^{123}I-MIBG defects seen in lobes without perfusion defects in our patients indicate that lung ^{123}I-MIBG uptake may be more sensitively impaired than perfusion. Damaged sympathetic neurons widely distributed in pulmonary airways and vessels due to regional hypoxia associated with smoking (*3,8,10,15,16,23*) also may reduce ^{123}I-MIBG uptake in PE, since part of the circulating ^{123}I-MIBG is trapped in the presynapses of these neurons (*12–14,16*). The observed occasional faint ^{123}I-MIBG radioactivity in lung lobes with nearly complete perfusion defects can be explained by the difference between nonparticulate ^{123}I-MIBG and particulate ^{99m}Tc-macroaggregated albumin.

TABLE 3
Comparison of Lung ^{123}I-MIBG Kinetic Parameters Between Controls and PE Patients

Parameter	Controls	PE patients	*P*
Early L/M ratio	4.10 ± 1.00	1.55 ± 0.58	<0.0001
Delayed L/M ratio	2.82 ± 0.90	1.51 ± 0.49	<0.0001
Washout rate	30.7% ± 14.0%	1.0% ± 7.2%	<0.0001

The decreased lung ^{123}I-MIBG washout rate in our patients may be partly caused by reduced perfusion associated with vascular damage. Although extracellular ^{123}I-MIBG increases because of decreased extraction of circulating ^{123}I-MIBG to damaged AECs and sympathetic neurons, decreased perfusion disrupts back-diffusion of this component to systemic circulation (*15,17,21*). Lack of integrity or dysfunction of AECs in PE patients also decreases the ^{123}I-MIBG washout rate, as various other lung disorders with injury of AECs persistently show a decreased ^{123}I-MIBG washout rate (*16, 18,20–23,34*).

The observed correlations of total-lung ^{123}I-MIBG uptake and washout rate with A-aDo_2 in our patients strengthen the value of ^{123}I-MIBG SPECT in assessing lung pathophysiology in PE. A-aDo_2 should be increased proportionally by the reduced surface and integrity of AECs. Recently, injury of AECs has been of great concern as the primary pathogenesis of smoking-induced PE (*1–11,31,35,36*). A recent ultrastructural study showed early disruption of AECs to be associated with smoking-induced chronic inflammatory processes and regional hypoxia (*1,3,31*). Decreased expression of vascular endothelial growth factor and its receptor is reported to enhance apoptosis of AECs, causing progressive disappearance of lung tissue in smoking-induced PE (*5,8,10,11,29, 30,35,36*).

TABLE 4
Linear Dependency of Total-Lung Early and Delayed L/M Ratios, Washout Rate, and Extent of Perfusion Defects and Low-Attenuation Areas on A-aDo_2 in PE Patients

Parameter	Formula	*R*	*P*
Early L/M ratio	$y = 34.147 - 8.569x$	0.406	0.0027
Delayed L/M ratio	$y = 32.204 - 7.51x$	0.363	0.029
Washout rate	$y = 22.042 - 1.18x$	0.833	<0.0001
Perfusion defects*	$y = 11.265 + 459x$	0.333	0.0471
Low-attenuation areas†	$y = 20.345 + 031x$	0.024	NS

*Percentage of total-lung voxels with radioactivity < 10% of maximum on perfusion SPECT.
†Percentage of total-lung voxels with attenuation < −960 HU on CT.
NS = not statistically significant.

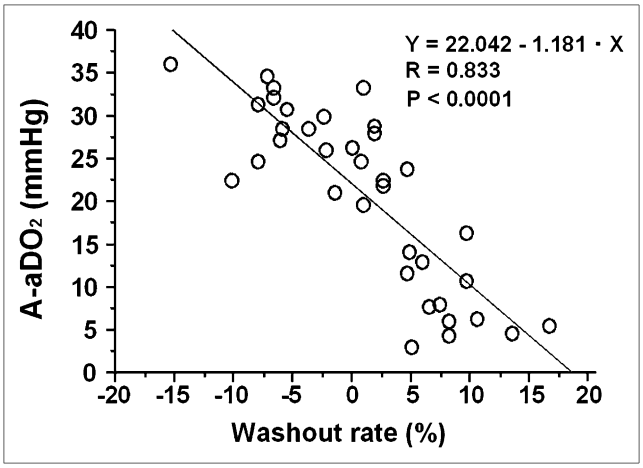

FIGURE 5. Correlation between total-lung ^{123}I-MIBG washout rate and A-aDo_2 in PE patients. Linear regression analysis shows significant reverse correlation in 36 PE patients.

The present finding of decreased lung ^{123}I-MIBG uptake and washout rate in PE patients is consistent with the recent pilot study of planar ^{123}I-MIBG scintigraphy, but the study evaluated only the upper lung zones, without comparison with lung perfusion, and showed correlations of lung ^{123}I-MIBG washout rate with the severity of emphysema on CT (*23*). Because ^{123}I-MIBG defects were occasionally seen without noticeable low-attenuation areas in our patients, CT may not be sufficiently sensitive to identify mild alveolar pathophysiology in PE (*27,37*).

The altered lung ^{123}I-MIBG uptake in our PE patients seems to be associated with smoking-induced pathologic changes in AECs, since smoking is a strong factor for injuring AECs (*2–4*). However, polluted air and some foods and drugs may also cause pathologic changes in AECs and altered ^{123}I-MIBG uptake. Further evaluation is required.

CONCLUSION

Impaired ^{123}I-MIBG uptake in the lungs of PE patients was evaluated in cross-sectional comparisons of ^{123}I-MIBG SPECT scans with perfusion SPECT scans and CT scans. Lung ^{123}I-MIBG uptake and washout rate were significantly lower in patients than in controls. Lung ^{123}I-MIBG uptake in these patients was frequently focally discordant with perfusion or morphologic abnormalities, as ^{123}I-MIBG defects were often more extensive than perfusion defects or low-attenuation areas and occasionally were seen even without noticeable perfusion defects or low-attenuation areas. The estimated total-lung ^{123}I-MIBG kinetic parameters were correlated with A-aDo_2 but not with the extent of perfusion defects or low-attenuation areas. ^{123}I-MIBG SPECT allows evaluation of lung pathophysiology in PE independently of perfusion SPECT or morphologic CT, and impairment of lung ^{123}I-MIBG uptake may be more extensive than perfusion or morphologic abnormalities in PE.

DISCLOSURE STATEMENT

The costs of publication of this article were defrayed in part by the payment of page charges. Therefore, and solely to indicate this fact, this article is hereby marked "advertisement" in accordance with 18 USC section 1734.

ACKNOWLEDGMENT

No potential conflict of interest relevant to this article was reported.

REFERENCES

1. Morissette MC, Parent J, Milot J. Alveolar epithelial and endothelial cell apoptosis in emphysema: what we know and what we need to know. *Int J Chron Obstruct Pulmon Dis.* 2009;4:19–31.
2. Ferrer E, Peinado VI, Díez M, et al. Effects of cigarette smoke on endothelial function of pulmonary arteries in the guinea pig. *Respir Res.* 2009;10:76–86.
3. Yang Q, Underwood MJ, Hsin MK, Liu XC, He GW. Dysfunction of pulmonary vascular endothelium in chronic obstructive pulmonary disease: basic considerations for future drug development. *Curr Drug Metab.* 2008;9:661–667.
4. Demedts IK, Demoor T, Bracke KR, Joos GF, Brusselle GG. Role of apoptosis in the pathogenesis of COPD and pulmonary emphysema. *Respir Res.* 2006;7:53–62.
5. Tuder RM, Yun JH. Vascular endothelial growth factor of the lung: friend or foe. *Curr Opin Pharmacol.* 2008;8:255–260.
6. Plataki M, Tzortzaki E, Rytila P, Demosthenes M, Koutsopoulos A, Siafakas NM. Apoptotic mechanisms in the pathogenesis of COPD. *Int J Chron Obstruct Pulmon Dis.* 2006;1:161–171.
7. Park JW, Ryter SW, Choi AM. Functional significance of apoptosis in chronic obstructive pulmonary disease. *COPD.* 2007;4:347–353.
8. Thébaud B, Abman SH. Bronchopulmonary dysplasia: where have all the vessels gone? Roles of angiogenic growth factors in chronic lung disease. *Am J Respir Crit Care Med.* 2007;175:978–985.
9. Taraseviciene-Stewart L, Douglas IS, Nana-Sinkam PS, et al. Is alveolar destruction and emphysema in chronic obstructive pulmonary disease an immune disease? *Proc Am Thorac Soc.* 2006;3:687–690.
10. Voelkel NF, Cool CD. Pulmonary vascular involvement in chronic obstructive pulmonary disease. *Eur Respir J Suppl.* 2003;46:28s–32s.
11. Kanazawa H, Hirata K, Yoshikawa J. Imbalance between vascular endothelial growth factor and endostatin in emphysema. *Eur Respir J.* 2003;22:609–612.
12. Lee KH, Ko BH, Paik JY, et al. Characteristics and regulation of I-123-MIBG transport in cultured pulmonary endothelial cells. *J Nucl Med.* 2006;47:437–442.
13. Slosman DO, Polla BS, Donath A. I-123-MIBG pulmonary removal; a biochemical marker of minimal lung endothelial cell lesions. *Eur J Nucl Med.* 1990;16:633–637.
14. Glowniak JV, Wilson RA, Joyce ME, Turner FE. Evaluation of metaiodobenzylguanidine heart and lung extraction fraction by first-pass analysis in pigs. *J Nucl Med.* 1992;33:716–723.
15. Glowniak JV, Kilty JE, Amara SG, et al. Evaluation of metaiodobenzylguanidine uptake by norepinephrine, dopamine and serotonin transporters. *J Nucl Med.* 1993;34:1140–1146.
16. Murashima S, Takeda K, Matsumura K, et al. Increased lung uptake of iodine-123-MIBG in diabetics with sympathetic nerve dysfunction. *J Nucl Med.* 1998;39:334–338.
17. Giordano A, Calcagni ML, Rossi B, et al. Potential use of iodine-123 metaiodobenzylguanidine radioaerosol as a marker of pulmonary neuroadrenergic function. *Eur J Nucl Med.* 1997;24:52–58.
18. Takabatake N, Arao T, Sata M, et al. Involvement of pulmonary endothelial cell injury in the pathogenesis of pulmonary fibrosis: clinical assessment by I-123-MIBG lung scintigraphy. *Eur J Nucl Med Mol Imaging.* 2005;32:221–228.
19. Urushihata K, Koizumi T, Hanaoka M, et al. Reduced lung uptake of iodine-123 metaiodobenzylguanidine in high-altitude pulmonary oedema. *Respirology.* 2008;13:897–902.
20. van Kroonenburgh M, Mostard R, Vöö S. Metaiodobenzylguanidine scintigraphy in pulmonary and cardiac disease. *Curr Opin Pulm Med.* 2010;16:511–515.
21. Unlü M, Inanir S. Prolonged lung retention of iodine-123-MIBG in diabetic patients. *J Nucl Med.* 1998;39:116–118.
22. Jonker GJ, Smulders NM, van Kroonenburgh MJ, et al. Lung-uptake and -washout of MIBG in sarcoidosis. *Respir Med.* 2008;102:64–70.
23. Arao T, Takabatake N, Sata M, et al. In vivo evidence of endothelial injury in chronic obstructive pulmonary disease by lung scintigraphic assessment of ^{123}I-metaiodobenzylguanidine. *J Nucl Med.* 2003;44:1747–1754.

24. American Thoracic Society. Standards for the diagnosis and care of patients with chronic obstructive pulmonary disease. *Am J Respir Crit Care Med.* 1995;152: 77–121.
25. Petty TL. COPD in perspective. *Chest.* 2002;121(5 suppl):116S–120S.
26. Sudoh M, Ueda K, Kaneda Y, et al. Breath-hold single-photon emission tomography and computed tomography for predicting residual pulmonary function in patients with lung cancer. *J Thorac Cardiovasc Surg.* 2006;131:994–1001.
27. Müller NL, Coxson H. Chronic obstructive pulmonary disease. 4: Imaging the lungs in patients with chronic obstructive pulmonary disease. *Thorax.* 2002;57:982–985.
28. Catravas JD, Lazo JS, Dobuler KJ, Mills LR, Gillis CN. Pulmonary endothelial dysfunction in the presence or absence of interstitial injury induced by intratracheally injected bleomycin in rabbits. *Am Rev Respir Dis.* 1983;128:740–746.
29. Kasahara Y, Tuder RM, Cool CD, Lynch DA, Flores SC, Voelkel NF. Endothelial cell death and decreased expression of vascular endothelial growth factor and vascular endothelial growth factor receptor 2 in emphysema. *Am J Respir Crit Care Med.* 2001;163:737–744.
30. Kasahara Y, Tuder RM, Taraseviciene-Stewart L, et al. Inhibition of VEGF receptors causes lung cell apoptosis and emphysema. *J Clin Invest.* 2000;106: 1311–1319.
31. Kanazawa H. Role of vascular endothelial growth factor in the pathogenesis of chronic obstructive pulmonary disease. *Med Sci Monit.* 2007;13:RA189–RA195.
32. Santos S, Peinado VI, Ramirez J, et al. Characterization of pulmonary vascular remodeling in smokers and patients with mild COPD. *Eur Respir J.* 2002; 19:632–638.
33. Yamato H, Sun JP, Churg A, Wright JL. Cigarette smoke induced emphysema in guinea pigs is associated with diffusely decreased capillary density and capillary narrowing. *Lab Invest.* 1996;75:211–219.
34. Inoue Y, Machida K, Honda N, Nishikawa J, Sasaki Y. Localized reduction in I-123-MIBG accumulation in the lung. *Radiat Med.* 1994;12:245–247.
35. Yasuo M, Mizuno S, Kraskauskas D, et al Hypoxia inducible factor-1α in human emphysema lung tissue. *Eur Respir J.* 2010;37:775–783.
36. Mura M, Binnie M, Han B, et al. Functions of type II pneumocyte-derived vascular endothelial growth factor in alveolar structure, acute inflammation, and vascular permeability. *Am J Pathol.* 2010;176:1725–1734.
37. Noma S, Moskowitz GW, Herman PG. Pulmonary scintigraphy in elastase-induced emphysema in pigs: correlation with high-resolution computed tomography and histology. *Invest Radiol.* 1992;27:429–435.